A REVIEW OF THE ACCURACY OF STRESS CONCENTRATION FACTORS

By

MATTHEW L. MAUK

Bachelor of Science in Mechanical Engineering

Oklahoma State University

Stillwater, Oklahoma

1999

Submitted to the Faculty of the
Graduate College of the
Oklahoma State University
in partial fulfillment of
the requirements for
the Degree of
MASTER OF SCIENCE
December, 2010

A REVIEW OF THE ACCURACY OF STRESS

CONCENTRATION FACTORS

Thesis Approved:

Dr. James K. Good

Thesis Adviser

Dr. Ronald D. Delahoussaye

Dr. Gary E. Young

Dr. Mark E. Payton

Dean of the Graduate College

ACKNOWLEDGMENTS

I would like to thank Dr. James K. Good, for his support and sponsorship of this thesis, for which it would not have been possible. I would also like to thank Dr. Ronald D. Delahoussaye and Dr. Gary E. Young for their time and contributions. I would be remiss if I didn't thank two very important people in my life, my parents. They have, without question, sacrificed much in helping me achieve my goals throughout life.

TABLE OF CONTENTS

Chapter Page

LIST OF TABLES

LIST OF FIGURES

CHAPTER I

INTRODUCTION

Throughout the course of the design process engineers must be vigilant about their design to be sure their designs don't fail under normal conditions of operation. During the design of their components they may encounter similar geometries on a regular basis. For instance, holes drilled in plates in tension. This type of geometry recurs on a regular basis and must be analyzed for potential failure. Because of the regularity of this geometry, stress concentration tables have been established to help speed the analysis of the geometry. No need to "reinvent the wheel". Engineering students are taught about this early in their education and allowed to use it throughout the course of their future careers. Reference books have been written that contain this information to make it readily available for the engineer or student. As with any reference data, it should be verified to be applicable to the application at hand, but due to deadlines, assumptions may be made that the data in the reference books is correct if time and resources are not available to verify the established data. Thus if the published data is incorrect it could lead to an unacceptable design flaw that may fail at the most inopportune time.

CHAPTER II

LITERATURE SURVEY

2.1 Literature

There are several sources for stress concentration values. Two general references are “Peterson’s Stress Concentration Factors” (Peterson’s) [12] and “Mechanical Engineering Design” (Shigley) [16]. These sources are readily available and used widely throughout industry and collegiate environments.

Mechanical Engineering Design is a textbook used by many Engineering schools for the instruction of machine design and the analysis needed to assure that those design meet the intended requirements. This text is used to introduce students to a few general forms of stress concentrations. Students can then apply their skills to other forms of geometry in their field of expertise.

As with any design there are certain features that repeat themselves throughout the design. For example, fillets are used in corners to reduce the stresses in a component with two intersecting structures. Grooves are cut into shafts to allow for O-rings to seal fluids from leaking past them into the environment were they may cause harm to humans or the environment. With the recurrence of these features, a graph can be selected from a reference [12, 16] to determine if a

localized stress in the area of a stress concentration will exceed the material capabilities in that application.

Peterson's Stress Concentration Factors is a reference book for Engineers and students concerned with increasing stresses at the intersection of changing geometries. As opposed to Shigley it delves deeper into the theory of stress concentrations. It also provides a much wider field of geometries to reference for structural analysis.

2.2 Research Objective

In some cases the stress concentrations provided by these references deviate. This report looks at the deviation in the plots for the semicircular edge notch. Two other cases are also compared, the transverse hole and the waist geometry.

The semicircular edge notch data from Shigley and Peterson's are compared in Figure 2.1. The figure shows that the values for Shigley are different than those of Peterson's. The Shigley data taken from [13] was based on theoretical calculations of "Theory of Notch Stress" [11], which were derived from the theory of elasticity. The Peterson's data was based on calculations by [9] and [10].

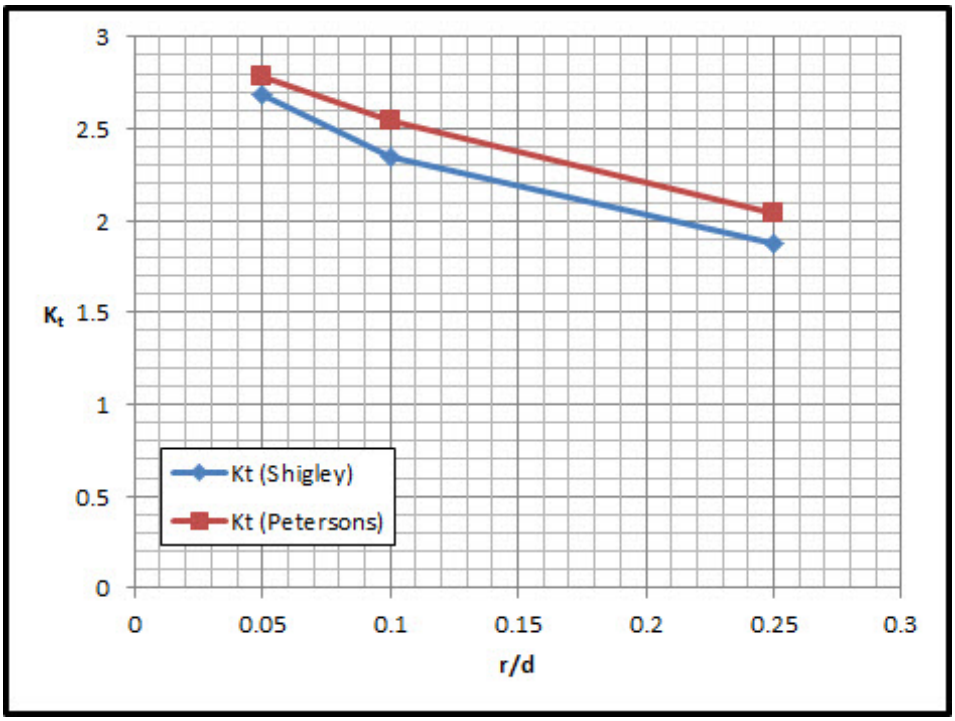

Figure 2.1 Semicircular Edge Notch Reference Comparisons

For the transverse hole configuration the comparison of the published sources shows good correlation of the data as seen in Figure 2.2. These results were based on photoelastic models. For Shigley's data source [15], the photoelastic measurements data was taken from [6] and [17]. The Peterson's data was based on theoretical calculations of a "successive approximation" for a tension problem [8].

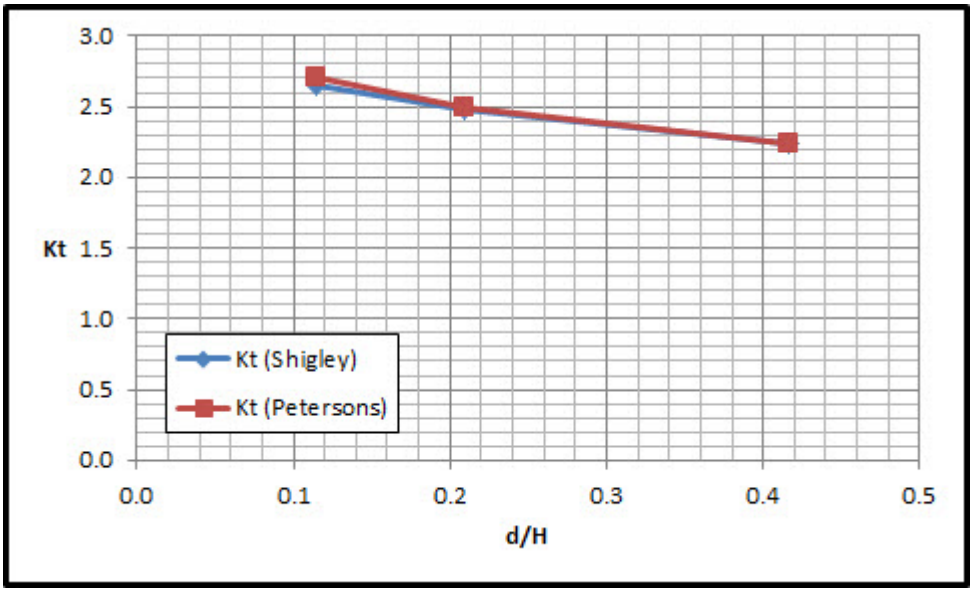

Figure 2.2 Transverse Hole Reference Comparisons

As seen in Figure 2.3 of the waist comparison, published sources are showing difference between their plotted values. The Shigley values were based on [14] whose values were taken from the photoelastic results of [6] and [7]. The Peterson's values were also based on photoelastic results [6] but included other refinements from [2] and [18], to improve the values for K_t as the original data was showing lower values [6].

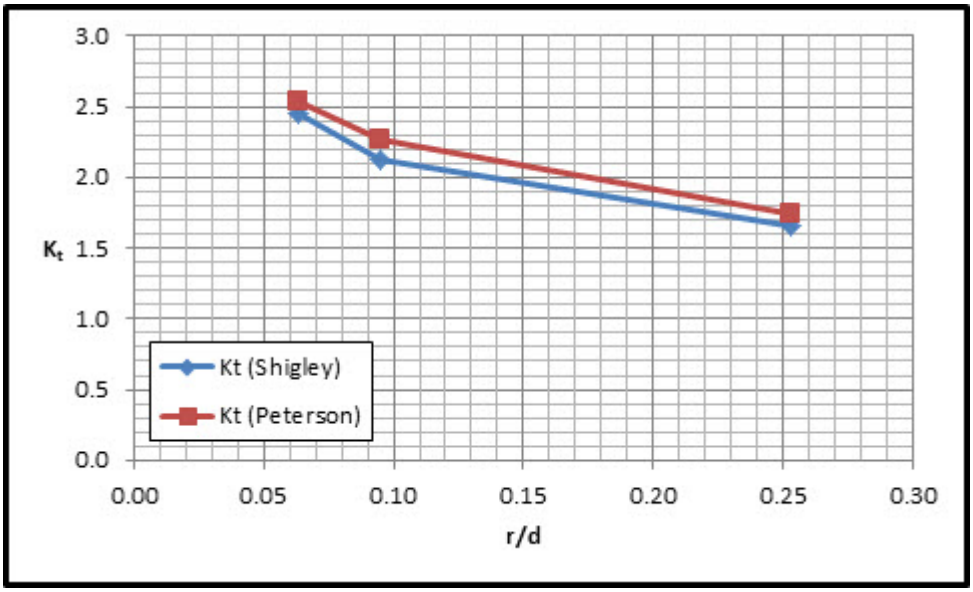

Figure 2.3 Waist Reference Comparisons

The three geometries are compared through different means of measurement. Photoelastic stress analysis is used for one type of analysis. The finite element method is used for the second type of analysis. These results will then be compared to the graphs in Shigley and Peterson's.

CHAPTER III

THE FINITE ELEMENT METHOD ATTACK

3.1 Introduction

The first method of attack on the stress concentration factors is Finite Element Analysis (FEA). FEA has become a common tool for many engineers in the past decade. Software has been written with them in mind to help further the designs they produce. It is a viable method of determining stress concentrations in complex geometries as well as simple geometries as is the case here. Abaqus was chosen as the software to perform these analyses. It is widely used in the automotive industry as well as other fields.

3.2 Software

To begin with, the geometry for analysis was modeled directly in the Abaqus 6.9.1 software itself. The graphical user interface (GUI), has a modest capability for modeling different geometries. It also has the capability of importing geometry directly from computer aided design (CAD) software as well. This wasn't necessary in this case as the geometry was simple and easy to create in the provided GUI. The geometry was modeled as a 2D surface. For the purposes of this report the measurements of the photoelastic models was used to better correlate between physical measurements and FEA results. The surface was then meshed using the CPS8R element [1], which is an 8 node plane stress element with reduced integration. The thickness of the geometry was controlled in the material section property.

3.3 Setup

For the given geometries, two of the three were modeled with quarter symmetry, transverse hole and edge notch. In the third case the waist samples were modeled using half symmetry. Then the material properties were applied to the model. For the PS-1 material the elastic modulus used for all samples was E=360,000 psi and a poison ratio of υ=0.38 [4].

The applied load was chosen based on keeping the maximum stress at the stress concentration below the yield point of the PS-1 material. The properties given [4] did not include yield strength. Typically yield strength is determined from a 0.2% strain offset of the elastic modulus and its intersect with the stress/strain plot. As an engineering judgment, the calculation of the yield strength will be calculated as 0.2% of the Elastic modulus (3.1). This value will be conservatively lower than the actual yield strength of the material.

$$\boldsymbol{S_y = E * 0.2\% = 360{,}000\ psi * 0.2\% = 720\ psi} \tag{3.1}$$

The initial testing load was set at 10 lbf. Based on this load and the smallest cross sectional area of sample 3 of the transverse hole, the maximum allowable stress concentration factor was calculated (3.3).

$$\sigma_{nom,max} = \frac{Force}{Area} = \frac{10\ lbf}{.844" * .119"} = 100\ psi \tag{3.2}$$

$$K_{t,max} = \frac{S_y}{\sigma_{nom,max}} = \frac{720\ psi}{100\ psi} = 7.2 \tag{3.3}$$

From the FEA results, all the samples show that the maximum stress will be below yield as all the calculated stress concentration values are below the maximum of 7.2. Finally, the load **P** as it is applied to the FEA model is uniformly distributed across the edge of the model, Figure 3.2.

3.4 Mesh convergence

For mesh convergence, the geometries were analyzed with several different mesh sizes to determine the best mesh size to meet convergence of the results at the stress concentration. Looking at the transverse hole as an example, the mesh size was set to a global value of .050 in for element size. The peak stress S11 was documented and then the mesh was refined in the area of the geometry in question. The graph below shows the peak stress results at the edge of the hole with respect to the different mesh densities. The percent difference between the global mesh size of .01 in and the combined mesh size of .01 in global / .005 in local, resulted in a 0.27% increase in recorded stress.

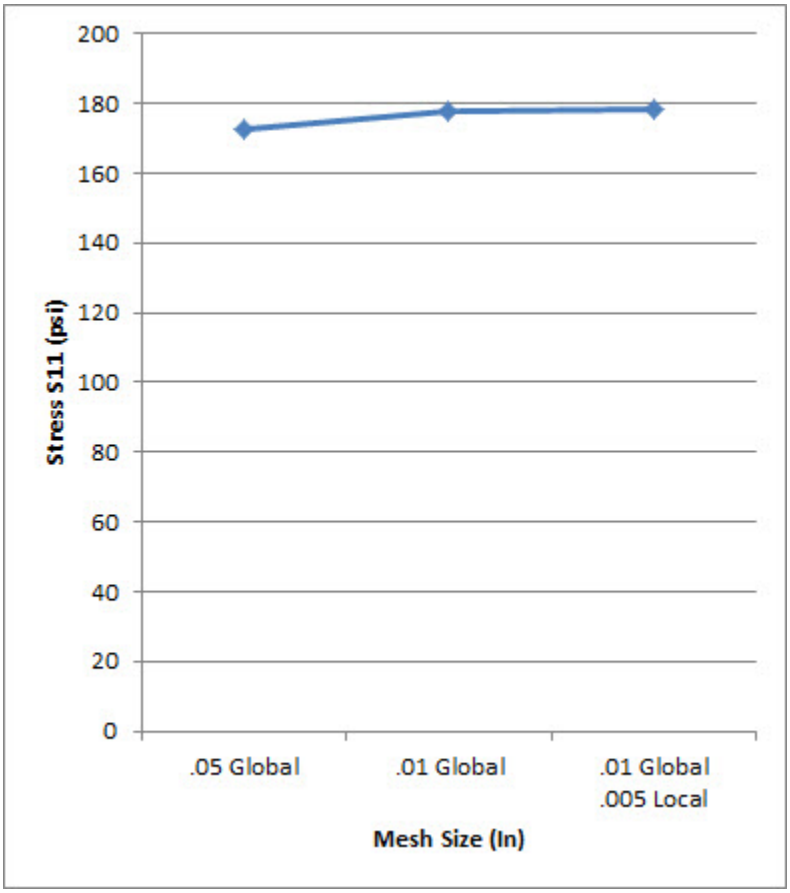

Figure 3.1 Mesh Convergence Graph.

The final mesh density selected for all analysis was a global value of .01 in and a local element size of .005 in. This resulted in an overall change in peak stress between a global of .01 in and a refined local of .005 in of 0.27%. Mesh and contour plots are located in Appendix A1. For all models an element type of 8-node biquadratic plane stress quadrilateral, reduced integration (CPS8R) was used [1]. The CPS8R element has two degrees of freedom in the X and Y directions at each node.

3.5 Results

The first sample analyzed was the transverse hole configuration. Three models for the different geometries given in Table 3.1 were developed. Symmetry was used in both the X and Y direction to simplify the model. The boundary conditions were set to symmetry on X and Y with a load P in the X direction, see Figure 3.2. Due to symmetry in the y direction the load was reduced in half to 5 lbf. The resulting values from the analysis are shown in Table 3.1. All contour plots are located in Appendix A2.

The stress concentration values K_t (3.4) are then calculated from the σ_{max} at the hole and divided by the net area stress σ_n (3.5).

$$Kt = \frac{\sigma_{\max}}{\sigma_n} \tag{3.4}$$

$$\sigma_n = \frac{Force}{net\_area} = \frac{Force}{(H-d)*t} \tag{3.5}$$

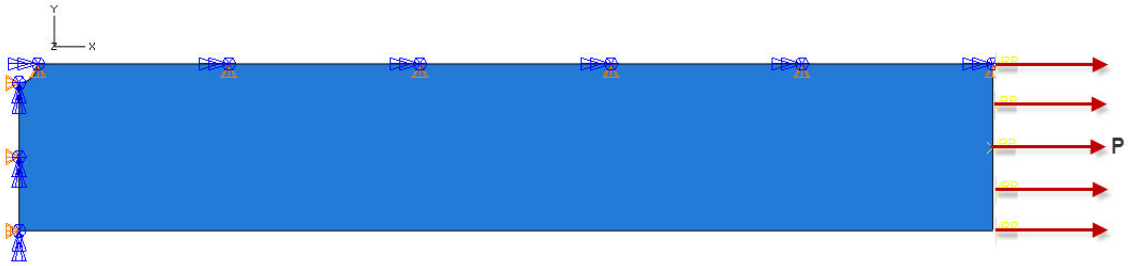

Figure 3.2 Transverse Hole Symmetry and Loading

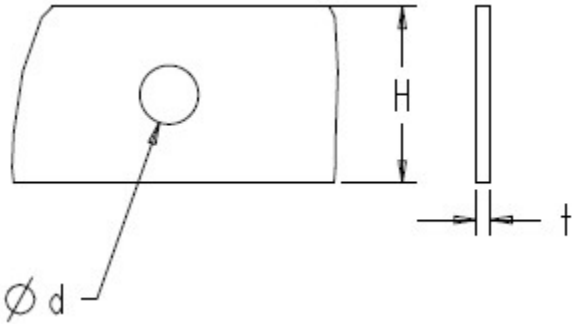

Figure 3.3 Transverse Hole Dimensions

Table 3.1 Transverse Hole Analysis Results and Gross Dimensions

Sample	d (in)	H (in)	t (in)	d/H	σ_{max} (psi)	σ_{n} (psi)	Kt
1	0.165	1.447	0.118	0.114	178.14	58.57	2.69
2	0.303	1.449	0.118	0.209	185.18	58.49	2.50
3	0.603	1.447	0.118	0.417	224.22	58.57	2.23

The next sample analyzed was the Semicircular Edge Notch configuration. The 3 different sized models were input into the software. The gross dimensions are given in Table 3.2. Symmetry was used in both the X and Y direction to simplify the model. The boundary conditions were set to symmetry on X and Y with a load P in the X direction, see Figure 3.4. Due to symmetry in the y direction the load was reduced in half to 5 lbf. The resulting values from the analysis are shown in Table 3.2. All contour plots are located in Appendix A2.

The stress concentration values K_t for the edge notch samples are calculated similar to the transverse hole with the exception of the σ_n which is calculated from equation (3.6).

$$\sigma_n = \frac{Force}{net\_area} = \frac{Force}{(H-2r)*t} \tag{3.6}$$

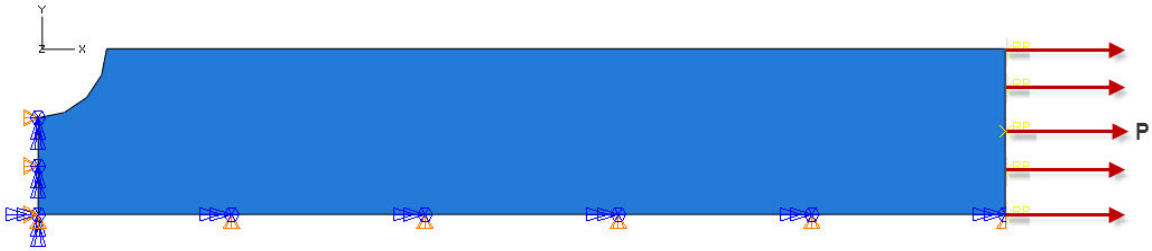

Figure 3.4 Semicircular Edge Notch Symmetry and Loading

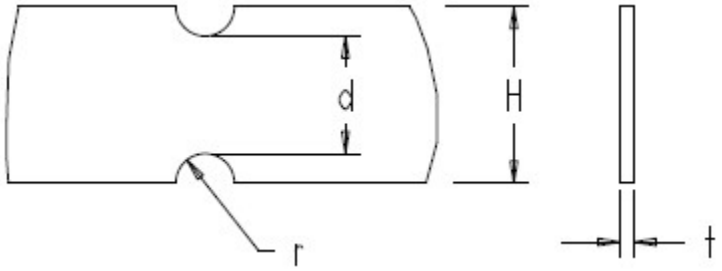

Figure 3.5 Semicircular Edge Notch Dimensions

Table 3.2 Semicircular Edge Notch Results and Gross Dimensions

Sample	r (in)	H (in)	d (in)	t (in)	2r/H	σ_{max} (psi)	σ_n (psi)	Kt
1	0.078	1.448	1.292	0.119	0.108	176.55	58.03	2.71
2	0.148	1.445	1.148	0.119	0.205	176.46	58.15	2.41
3	0.297	1.451	0.857	0.119	0.409	180.90	57.91	1.85

Finally the last sample analyzed was the Waist configuration. The 3 different sized models were input into the software. The gross dimensions of the models are given in Table 3.3. Symmetry was used in the Y direction to simplify the model. The boundary conditions were set to

symmetry on Y with a load P in the X direction, see Figure 3.6. Due to symmetry in the y direction the load was reduced in half to 5 lbf. The resulting values from the analysis are shown in Table 3.3. All contour plots are located in Appendix A2.

The stress concentration K_t (3.1) of the waist configuration is calculated straight from the measured σ_{max} and σ_n. Where σ_n is measured in the field of width d.

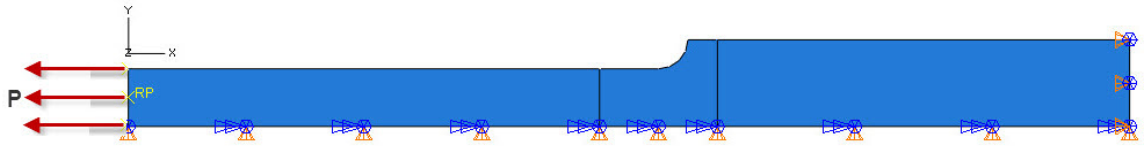

Figure 3.6 Waist Symmetry and Loading

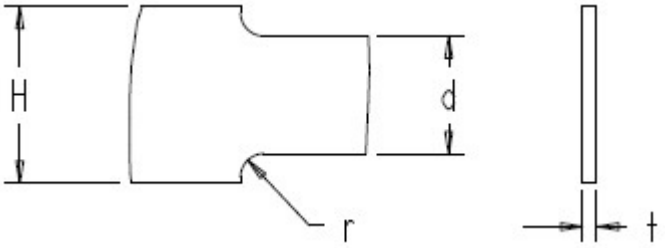

Figure 3.7 Waist Dimensions

Table 3.3 Waist Results and Gross Dimensions

Sample	r (in)	H (in)	d (in)	t (in)	H/d	r/d	σ_{max} (psi)	σ_n (psi)	Kt
1	0.063	1.483	0.986	0.119	1.504	0.063	56.67	85.23	2.49
2	0.094	1.484	0.990	0.119	1.499	0.095	56.63	84.88	2.21
3	0.250	1.487	0.988	0.119	1.505	0.253	56.51	85.05	1.69

CHAPTER IV

THE PHOTOELASTIC METHOD ATTACK

4.1 Introduction

Photoelastic stress analysis is a unique form of structural analysis. It involves the use of light passing through a plastic material that exhibits temporary double refraction, "optically isotropic when free of stress but becomes optically anisotropic and display characteristics similar to crystals when they are stressed" [3]. The light from the plastic is then passed through polarized plates. The resulting vision is one of a fringe pattern that describes the stresses in the material it is passing through. Decades ago these techniques were used in place of cumbersome FEA software and even before computers were available to analyze 2 dimensional models. It is considered more of an analog structural analysis versus today's high end computer based digital analysis.

4.2 Setup

For the photoelastic analysis, 9 different samples were produced to compare with other sources of data. The sample were broken into 3 groups, transverse hole, semicircular edge notch and waist. Within each group three different sized samples were produced to cover a broad range of geometry ratios.

Each sample was placed in an apparatus to apply a predefined load of 10 lbf. A load transducer was used to verify the correct force was applied. A polariscope was used to measure the stress level in the reduced width field of the sample and the peak stress at the stress concentration. From here the stress concentration factor K_t (4.1) can be calculated [12]. K_t is max normal stress divided by normal stress based on net area.

$$Kt = \frac{\sigma_{\max}}{\sigma_n} \tag{4.1}$$

Each sample was measured 5 times consecutively. Data was then averaged to obtain the results. The peak stress level was measured on both sides of the part and then averaged together to get a mean value. This was done to average out any bias from one side of the part to the other based on any non-symmetry of the machining.

4.3 Samples and Geometry

The machining methods are given in detail in Appendix A3.

The material used for the machined samples was a high-modulus polymer PS-1 [4]. The material was chosen for its ease of machining. The PS-1 properties are; Elastic Modulus E=360,000 psi, Poisson's ratio υ=0.38 and for these samples a general thickness of 0.120 inches with a tolerance of +/-0.002 inches. The sheets were received with a silver backing and a protective paper covering on the opposing side.

Figure 4.1 shows the base configuration of the specimens which was specified to be 10 inches by 1.500 inches, with two .375 inch holes 8.5 inches on center. The thickness was a predefined value based on the purchased material. Each sheet had its own specific thickness (t). The samples were machined in accordance with the machining process in Appendix A3. The final sample configuration is shown in Table 4.1, 9 samples in all.

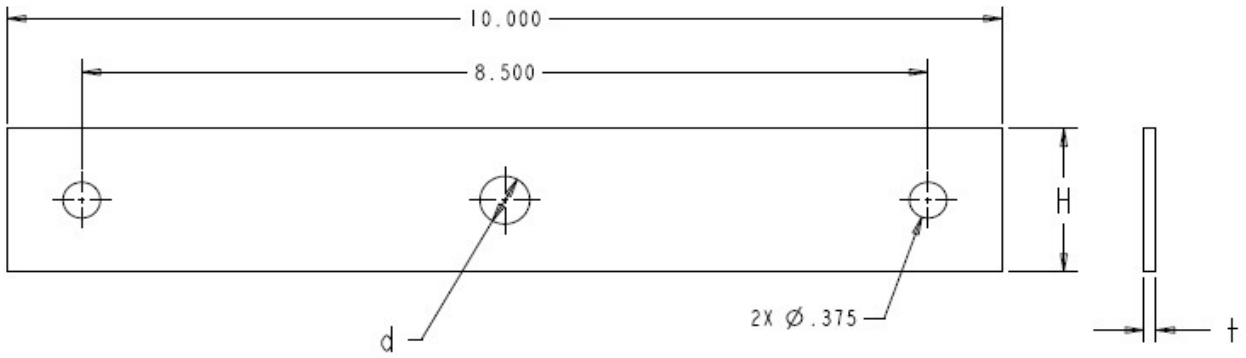

(a)

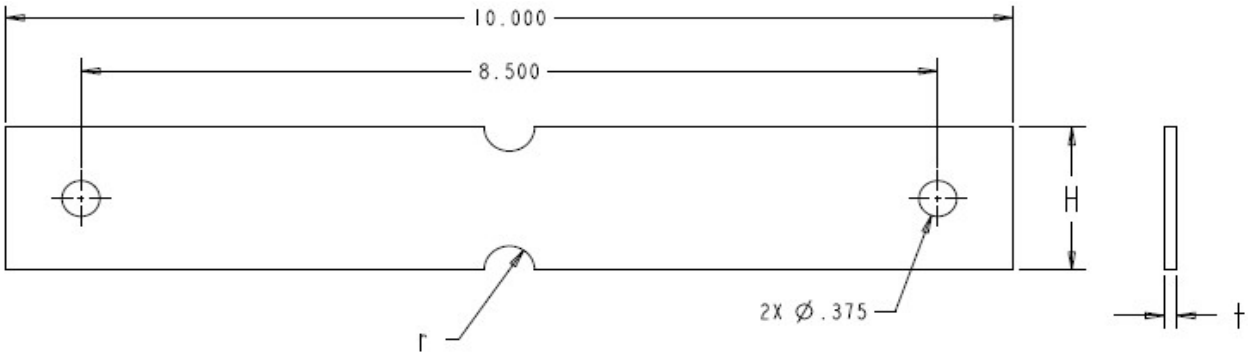

(b)

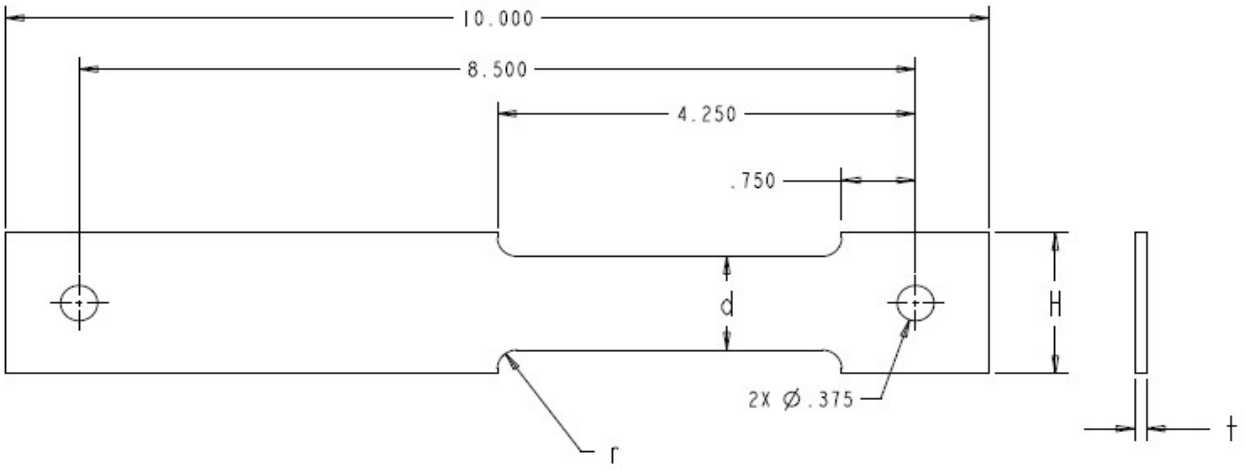

(c)

Figure 4.1 General Specimen Dimension used for (a) Transverse Hole (b) Semicircular Edge Notch (c) Waist

Table 4.1 Parameters for Specific Sample Geometries

Configuration		Width of Sample (in)	Width of Waist (in)	Diameter (in)	Radius (in)
		H	d	d	r
Transverse Hole	1	1.500	-	5/32	-
	2	1.500	-	19/64	-
	3	1.500	-	19/32	-
Semi Circular Edge Notch	1	1.500	-	-	5/64
	2	1.500	-	-	19/128
	3	1.500	-	-	19/64
Waist	1	1.500	1.000	-	5/64
	2	1.500	1.000	-	19/128
	3	1.500	1.000	-	19/64

4.4 Results

The first sample analyzed was the transverse hole configuration. The samples were measured with digital calipers in order to confirm their actual size listed in Table 4.2. Then measurements were taken with the polariscope to obtain $\sigma_{max,avg}$, which is read from the outer edge of the hole. From here σ_n (4.2) was calculated to determining K_t.

$$\sigma_n = \frac{Force}{net\_area} = \frac{Force}{(H-d)*t} \tag{4.2}$$

Table 4.2 Transverse Hole Photoelastic Results and Gross Dimensions

Sample	d (in)	H (in)	t (in)	d/H	$\sigma_{max.avg}$ (psi)	σ_n (psi)	$K_{t,avg}$	$K_{t,avg}$ Std Err
1	0.165	1.447	0.118	0.114	191.6	65.94	2.9	0.015
2	0.303	1.449	0.118	0.209	194.6	73.91	2.6	0.027
3	0.603	1.447	0.118	0.417	240.8	99.57	2.4	0.015

For the semicircular edge notch samples, K_t is calculated very similar to that of the transverse hole. $\sigma_{max,avg}$ is read from the inner edge of the notch and σ_n is calculated from the net area (4.3). Results are shown in Table 4.3

$$\sigma_n = \frac{Force}{net\_area} = \frac{Force}{(H-2r)*t} \tag{4.3}$$

Table 4.3 Semicircular Edge Notch Photoelastic Results and Gross Dimensions

Sample	r (in)	H (in)	d (in)	t (in)	r/d	2r/H	$\sigma_{max,avg}$ (psi)	σ_n (psi)	$K_{t,avg}$	$K_{t,avg}$ Std Err
1	0.078	1.448	1.292	0.119	0.060	0.108	182.7	65.05	2.8	0.009
2	0.148	1.445	1.148	0.119	0.129	0.205	169.7	73.19	2.3	0.016
3	0.297	1.451	0.857	0.119	0.346	0.409	211.8	98.03	2.2	0.022

Finally the results for the waist samples are given in Table 4.4. This case gives $\sigma_{n,avg}$ as a measured value as opposed to being calculated like the other samples. The reduced section of width d is the nominal net area needed for the calculations of K_t.

Table 4.4 Waist Photoelastic Results and Gross Dimensions

Sample	r (in)	H (in)	d (in)	t (in)	H/d	r/d	$\sigma_{max,avg}$ (psi)	$\sigma_{n,avg}$ (psi)	$K_{t,avg}$	$K_{t,avg}$ Std Err
1	0.063	1.483	0.986	0.119	1.504	0.063	205.4	84.6	2.4	0.032
2	0.094	1.484	0.990	0.119	1.499	0.095	186.0	85.4	2.2	0.043
3	0.250	1.487	0.988	0.119	1.505	0.253	175.8	86.6	2.0	0.040

4.5 Errors

As with any project that requires human interaction or machines designed and built by humans there will be errors in the research results. Photoelastic analysis is no different and the following errors were identified.

The first errors were introduced during the machining process. The samples were specified to have a predefined size as seen in Figure 4.1 with dimension from Table 4.1. Due to wear in the machining equipment and error on the machinist's part, the specimens' final sizes were not what was initial specified. More care should be taken by the machinist to minimize human error and newer equipment with Computer Numerical Control is recommended.

For these samples the final sample dimension can be seen in Tables 4.2, 4.3, 4.4. These dimensions were taken with a digital caliper with resolution to .001 inches. Some features presented difficulties to measure, such as the edge notch and the fillet radius in the waist samples. These features were assumed to be of nominal size. These features could be under or oversized. To correct this, it is recommended to have the samples measured by a Coordinate Measurement Machine. These would provide final dimensional data of the samples to minimize any calculated error to be compared with the measured photoelastic data.

The next place error was introduced into the results was during the stress measurements. Here there is the potential for equipment error as well as human error. The measurement equipment was calibrated before the measurements were taken so any error there will be ignored. The human error deals with the viewing of the fringes and the measurement point of the peak stress. During the process the operator is adjusting the equipment to the point of termination of the black fringes at the stress point. The first error here is the point at which the fringe disappears. This point is open to interpretation by the operator, it was noticed that eye fatigue also played a part in the difficulty of making the measurements. The next issue was the orientation of the sample. The sample was being viewed on opposing sides and any rotation of the sample with respect to the polariscope would show the machined edge directly or make it visible threw the plastic, thus adding to the difficultly of read the extinction of the black fringe. The standard error was quantified and listed in Tables 4.2, 4.3, 4.4.

CHAPTER V

COMPARISON OF RESULTS

The following graphs compare the values for K_t from the 4 different sources. The data plotted for Peterson's and Shigley was interpolated from the graphs located in their respective books. There is a small amount of error present in these data sets represented here as human error factors into the interpolations of the graphs. A machinist ruler was used to measure the distance between major gridlines and interpolate to the closest values.

5.1 Transverse Hole

Figure 5.1 shows the data plots for Peterson's, Shigley, FEA and photoelastic samples. There is good correlation between Peterson's, Shigley and FEA results. At the lower d/H value (sample 1) there is a small amount of deviation from Shigley, which could be the result of interpolation error. The data for the photoelastic specimens parallel the results but show a higher K_t values and thus only provide comparison based on trend. The error bars for the FEA results have not been shown as the error is much less than the photoelastic models.

Figure 5.1 Transverse Hole Results Comparison

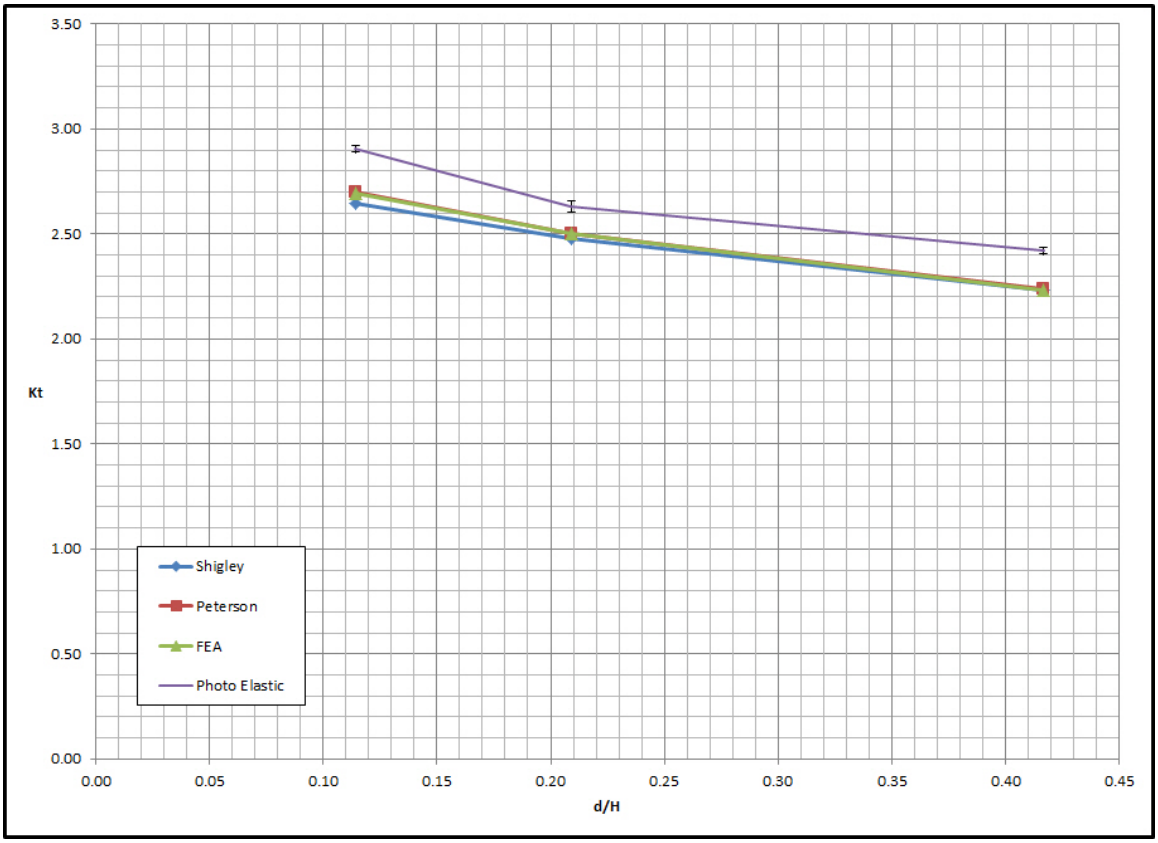

5.2 Semicircular Edge Notch

The semicircular edge notch results show good correlation between FEA results and data interpolated from Peterson's. Shigley is significantly lower than those two data sets, refer to Figure 5.2. There is a slight departure between the two at the midpoint, which is a potential error in the interpretation of the graph from Peterson's. The photoelastic results do not follow the data of the other two results and thus cannot be used for comparison.

Figure 5.2 Semicircular Edge Notch Results Comparison

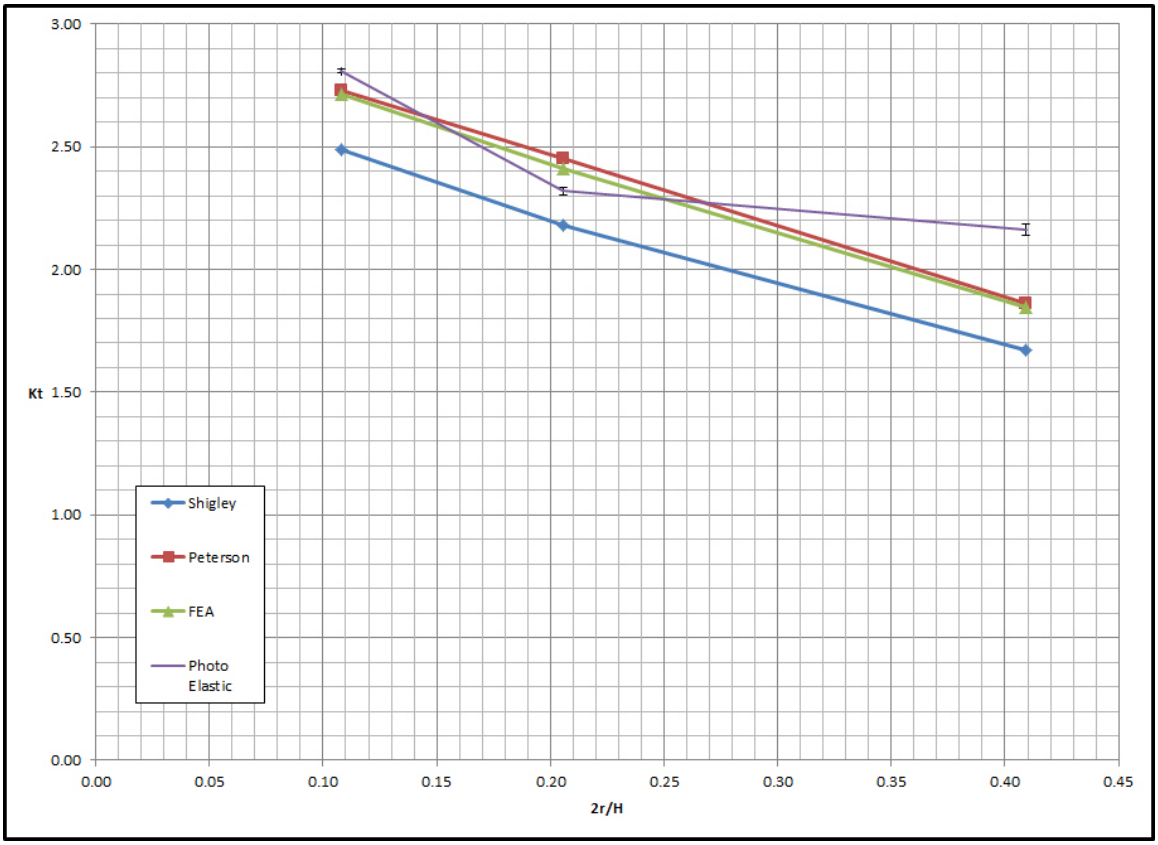

5.3 Waist

Finally, the waist data presented in Figure 5.3 shows correlation among Peterson's, Shigley and FEA. There is a small amount of shift in the K_t values at each of the data points; this is most likely a result of how the data was obtained for each source. The photoelastic results again show some discrepancies compared with the other data sources. At lower values of K_t the photoelastic models show a general correlation but for the higher r/d value results in a flyer compared to the rest of the data. Both Peterson's and Shigley's data are derived from photoelastic tests results; the Peterson's date has been refined as the original values were showing lower results. As well, some of the difference between these two sources, seen in Figure 5.3, may be the result of

interpolation error from the plots. It should be noted that the plot in Shigley is significantly smaller compared to Peterson's, thus presenting the possibility for more error in interpolation.

Figure 5.3 Waist Results Comparison

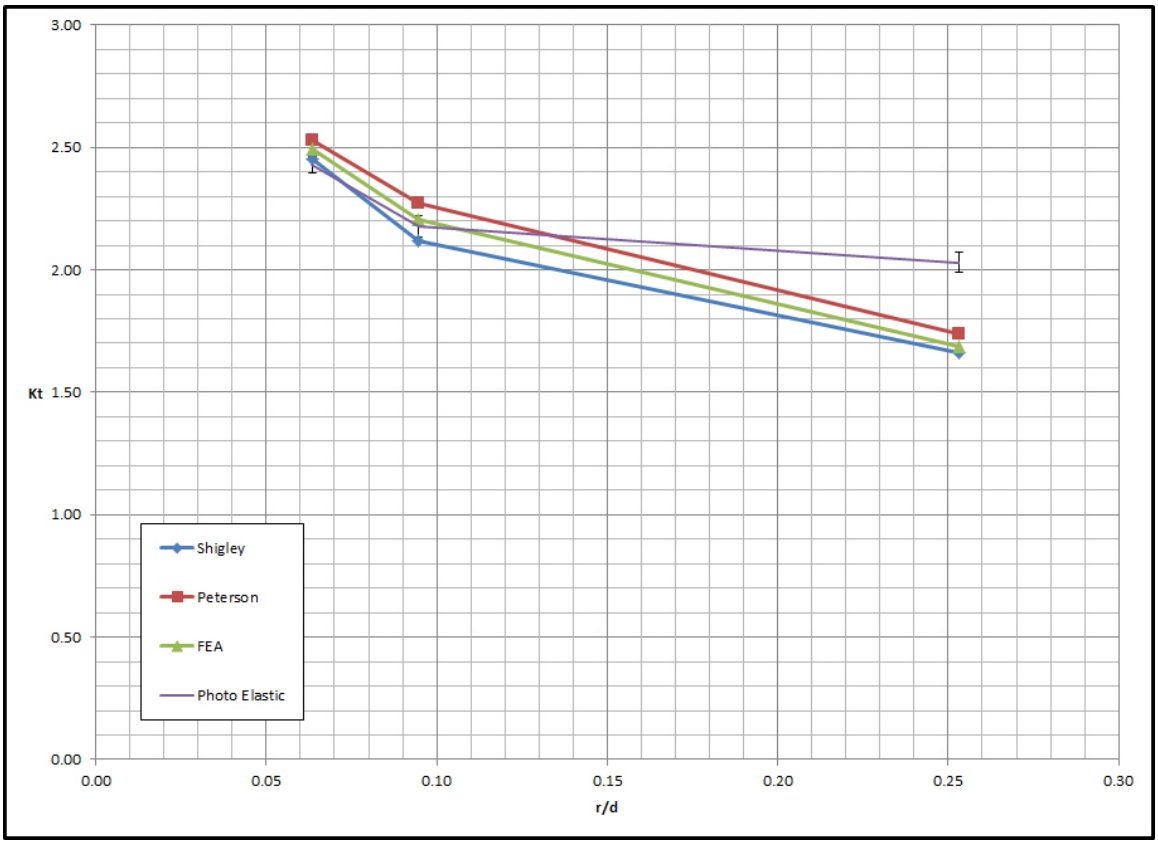

CHAPTER VI

CONCLUSIONS

The results for the transverse hole geometry shows good correlation between Peterson's, Shigley and FEA results. There is a small deviation in Shigley at the lower d/H, but that may be attributed to interpolation error of the graph. The photoelastic model has a similar trend, but the K_t values are higher.

The semicircular edge notch case presents the most significant error between the published sources. In Figure 5.2 it was shown that Shigley's K_t values were significantly lower than Peterson's and FEA results. This shows a level of error in the theoretical calculations used to create the plots. Results for the photoelastic samples again show a variation across the board and cannot be used as a comparison. FEA results correlated well to the data from Peterson's.

The last configuration looked at was the waist geometry. There are comparable trends among the plots for Peterson's, Shigley and FEA results. Though there is a shift in values between all three sources as seen in Figure 5.3. Both Peterson's and Shigley values are based from the same photoelastic results, though Peterson's has refined the values based on newer sources, as the original K_t values had been shown to be low. Photoelastic results are markedly better in this geometry at the lower r/d levels but sample 3 is a flyer, as its K_t result is significantly higher.

Through analysis it has been shown that the stress concentration results published in Shigley, for the semicircular edge notch, are in error compared with Peterson's and FEA analysis. The stress concentration values for the transverse hole geometry compare well, Figure 5.1. Finally, the waist geometry shows good trends but there is a small shift in the values between both published data and the FEA results. Photoelastic results can provide acceptable results when great care is taken to produce and measure the samples. This researcher's photoelastic results show significantly different values from published data and FEA results in most cases. These errors are attributed to the accuracy of the machining and the human error in data acquisition.

Photoelastic results for this report have shown that it can be significantly impacted by human error and that it requires a high level of accuracy and control in machining and reading the fringe results. Photoelastic measurement can be used to determine stress concentration values but great care is needed to assure good data. FEA is an excellent alternative that can be used in the future to calculate K_t values. In the past FEA was sophisticated software that required significant knowledge to obtain satisfactory results. As the software has matured the necessity of being an expert in it has subsided. It can provide an acceptable level of results to quantify and correlate results for stress concentration factors with basic knowledge of the software.

REFERENCES

1) *Abaqus Analysis User's Manual*, Version 6.9, Vol. 4, 2009.

2) Appl, F. J., and Koerner, D. R., "Stress concentration factors for U-shaped, hyperbolic and rounded V-shaped notches", *ASME Pap.* 69-DE-2, 1969, American Society of Mechanical Engineers, New York.

3) Dally, J. W., and Riley, W. F., *Experimental Stress Analysis*, 3rd ed., McGraw Hill 1991.

4) Document No. 11222, "PhotoStress Coating Materials and Adhesives", Micro-Measurements, 2010 March 29. <http://www.micro-measurements.com>

5) Document No. 11223, "Instructions for Bonding Flat and Contoured PhotoStress Sheets", Micro-Measurements. 2007 December 03. <http://www.micro-measurements.com>

6) Frocht, M. M., "Factors of stress concentration photoelastically determined", *Trans. ASME Appl. Mech. Sect*., 1969, Vol. 57, p. A-67.

7) Frocht, M. M., and Landsberg, D., "Factors of stress concentration in bars with deep sharp grooves and fillets in torsion", *Trans. ASME Appl. Mech. Sect.*, 1951, Vol. 73, p. 107.

8) Howland, R. C. J., "On the stresses in the neighborhood of a circular hole in a strip under tension", *Philos. Trans.R. Soc.(London) Ser. A*, 1929-1930, Vol. 229, p. 67.

9) Isida, M., "On the tension of the strip with semi-circular notches", *Trans. Jpn. Soc. Mech. Eng.*, 1953, Vol. 19, p. 5.

10) Ling, C.-B., “On stress concentration factor in a notched strip”, *Trans. ASME Appl. Mech. Sect.*, 1968, Vol. 90, p. 833.

11) Neuber, H., 1937, *Kerbspannungslehre*, Springer, Berlin; translation, 1945, *Theory of Notch Stress*, J.W. Edwards Co., Ann Arbor, MI 1946.

12) Pilkey, W. D., and Pilkey, D. F. *Peterson’s Stress Concentration Factors*, 3rd ed., John Wiley & Sons, Inc. 2007.

13) Peterson, R. E., Design Factors for Stress Concentration, *Machine Design*, 1951, Vol. 23, no. 3, p. 161.

14) Peterson, R. E., Design Factors for Stress Concentration, *Machine Design*, 1951, Vol. 23, no. 6, p. 173.

15) Peterson, R. E., Design Factors for Stress Concentration, *Machine Design*, 1951, Vol. 23, no. 7, p. 155.

16) Shigley, J. E., and Mischke, C. R., *Mechanical Engineering Design*, 5th ed., McGraw Hill, 1989.

17) Wahl, A. W., and Beeuwkes, R., “Stress concentration produced by holes and notches”, *Trans. ASME Appl. Mech. Sect.*, 1934, Vol. 56, p. 617.

18) Wilson, I. H., and White, D. J., “Stress concentration factors for shoulder fillets and grooves in plates”, *J. of Strain Anal.*, 1973, Vol. 8, p. 43.

APPPENDICES

A1 – FEA Mesh convergence

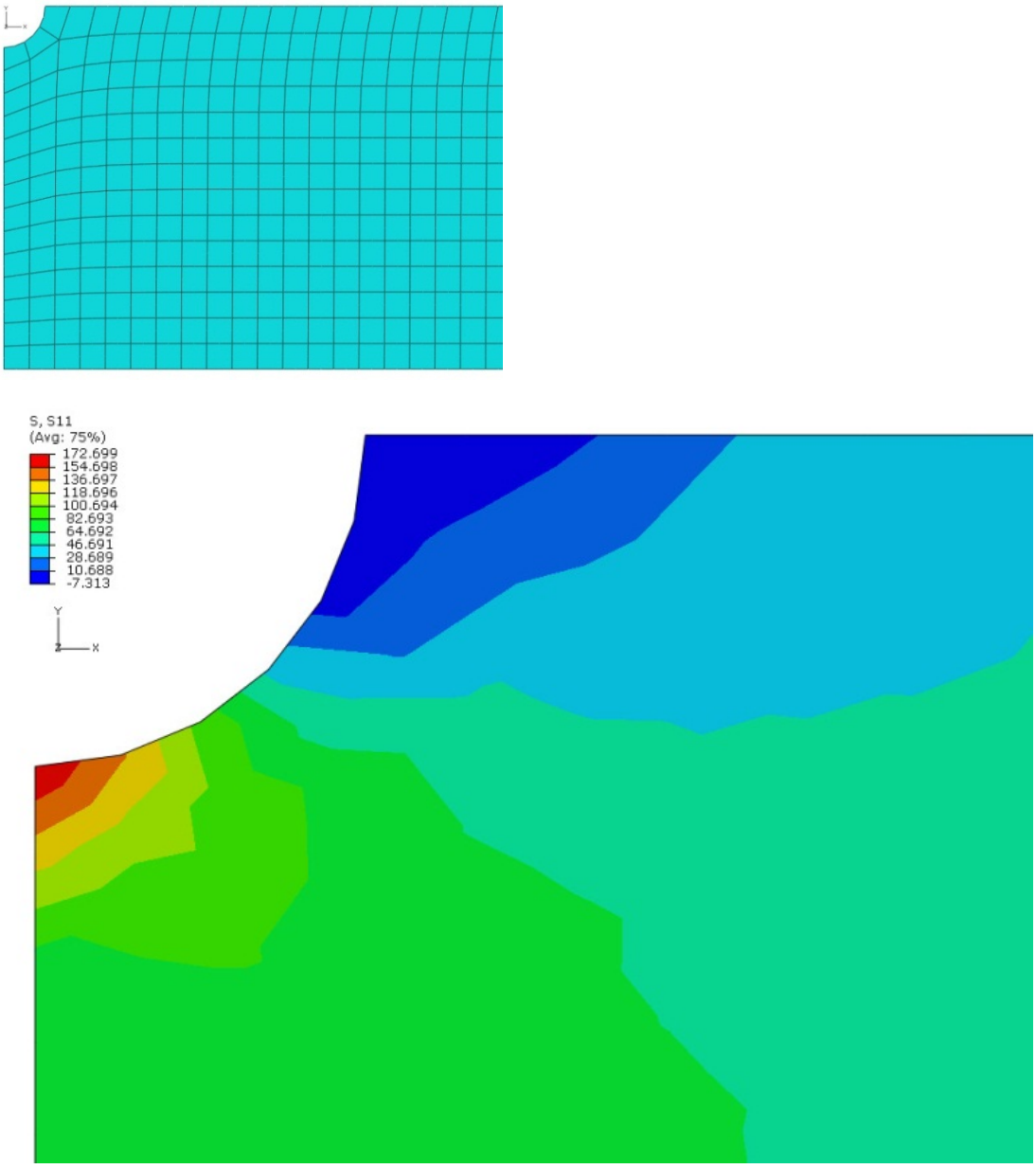

Figure 1 - Mesh size global .05

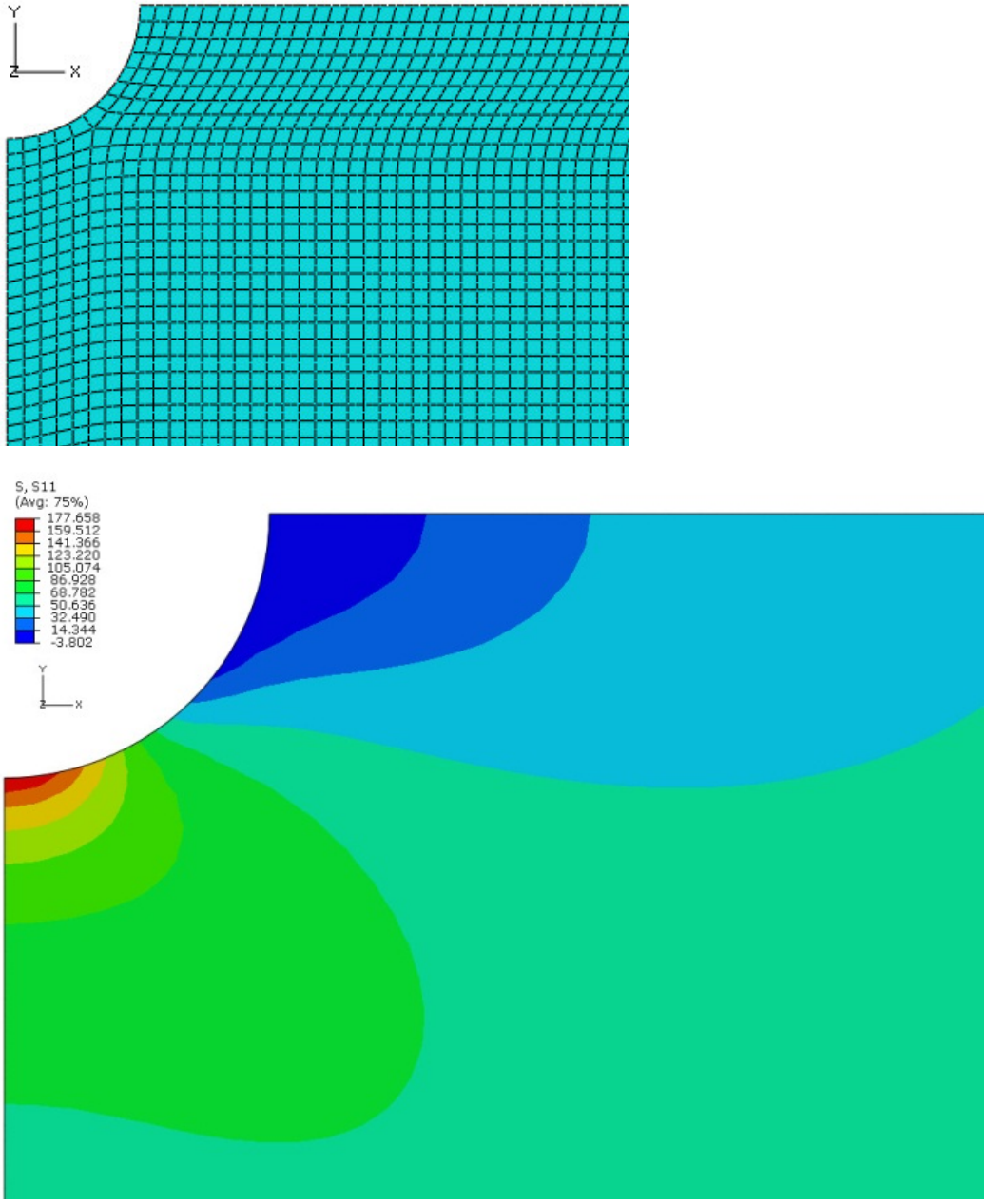

Figure 2 - Mesh size global .01

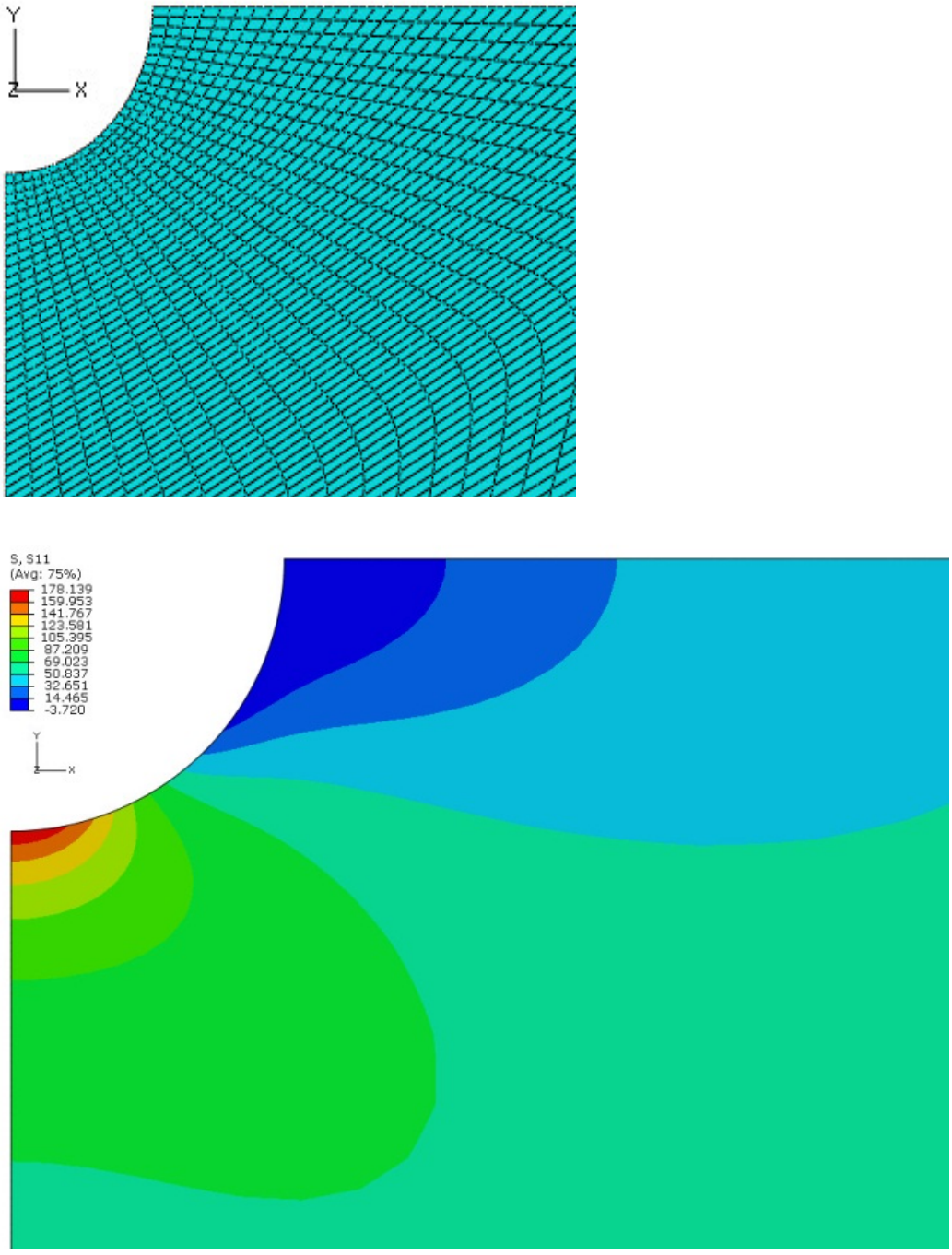

Figure 3 - Mesh size global .01 / local .005

A2 – FEA Results

Hole 1

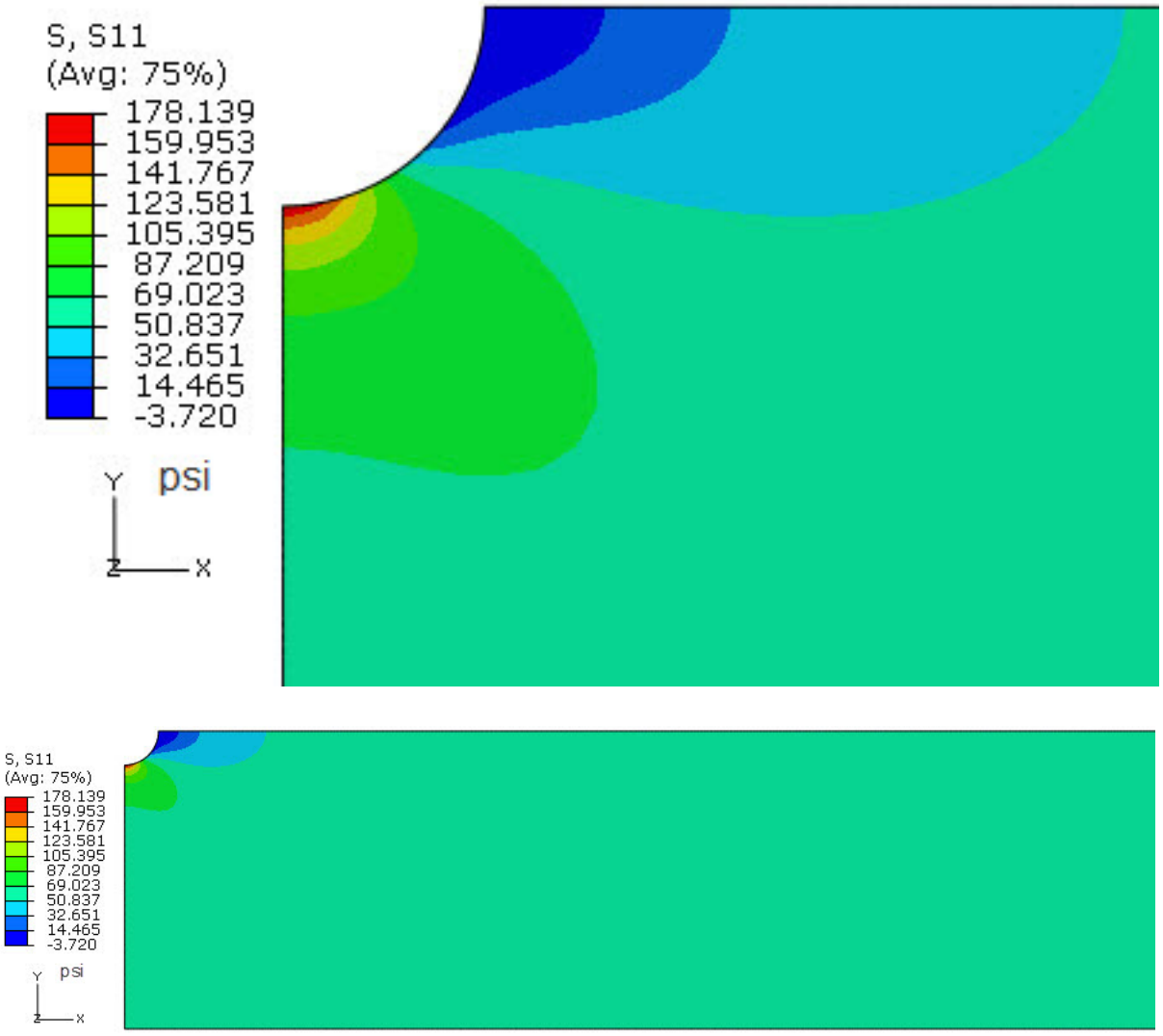

Hole 2

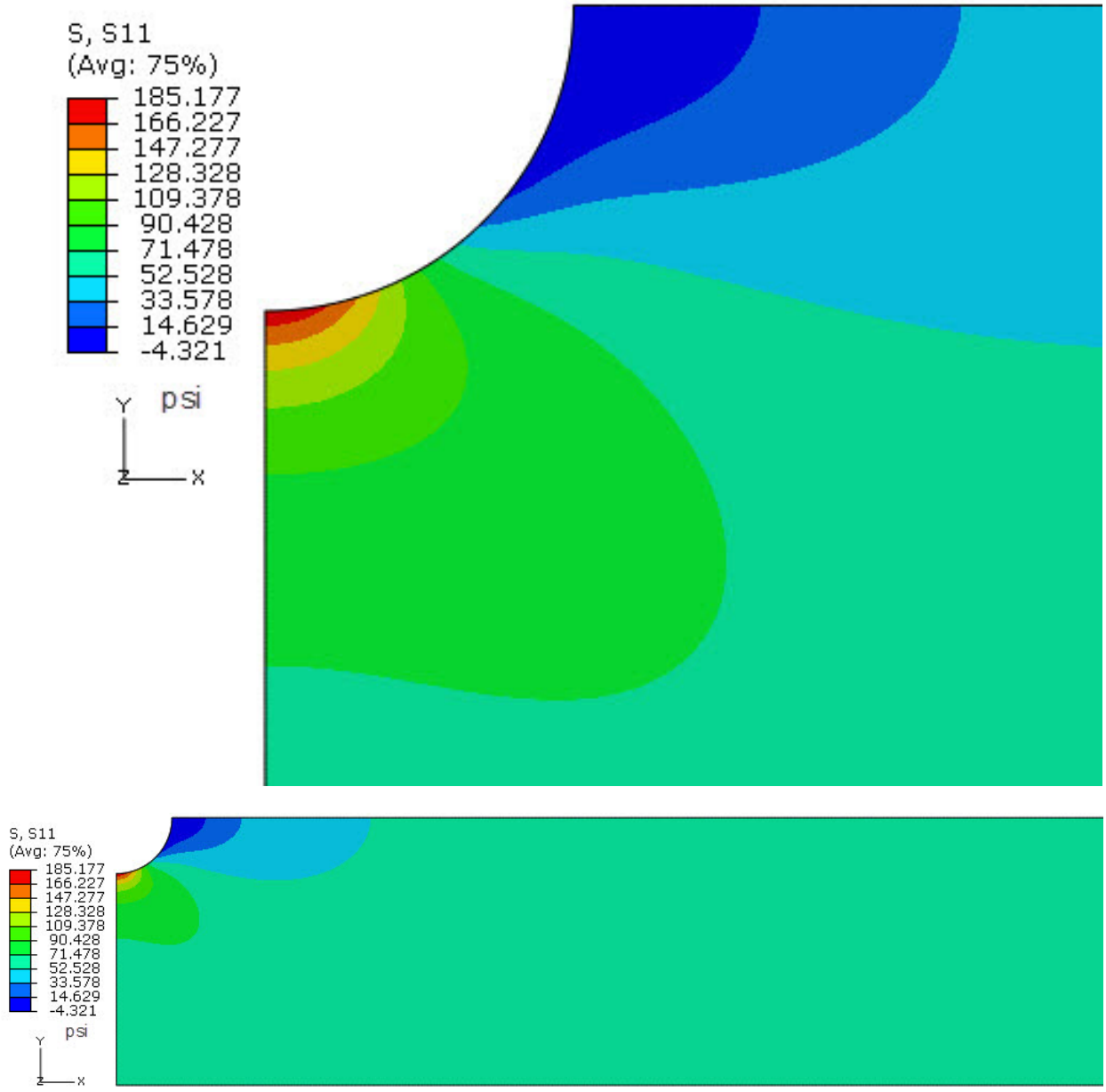
S, S11
(Avg: 75%)
185.177
166.227
147.277
128.328
109.378
90.428
71.478
52.528
33.578
14.629
-4.321
psi
Y
Z
X
S, S11
(Avg: 75%)
185.177
166.227
147.277
128.328
109.378
90.428
71.478
52.528
33.578
14.629
-4.321
psi
Y
Z
X

Hole 3

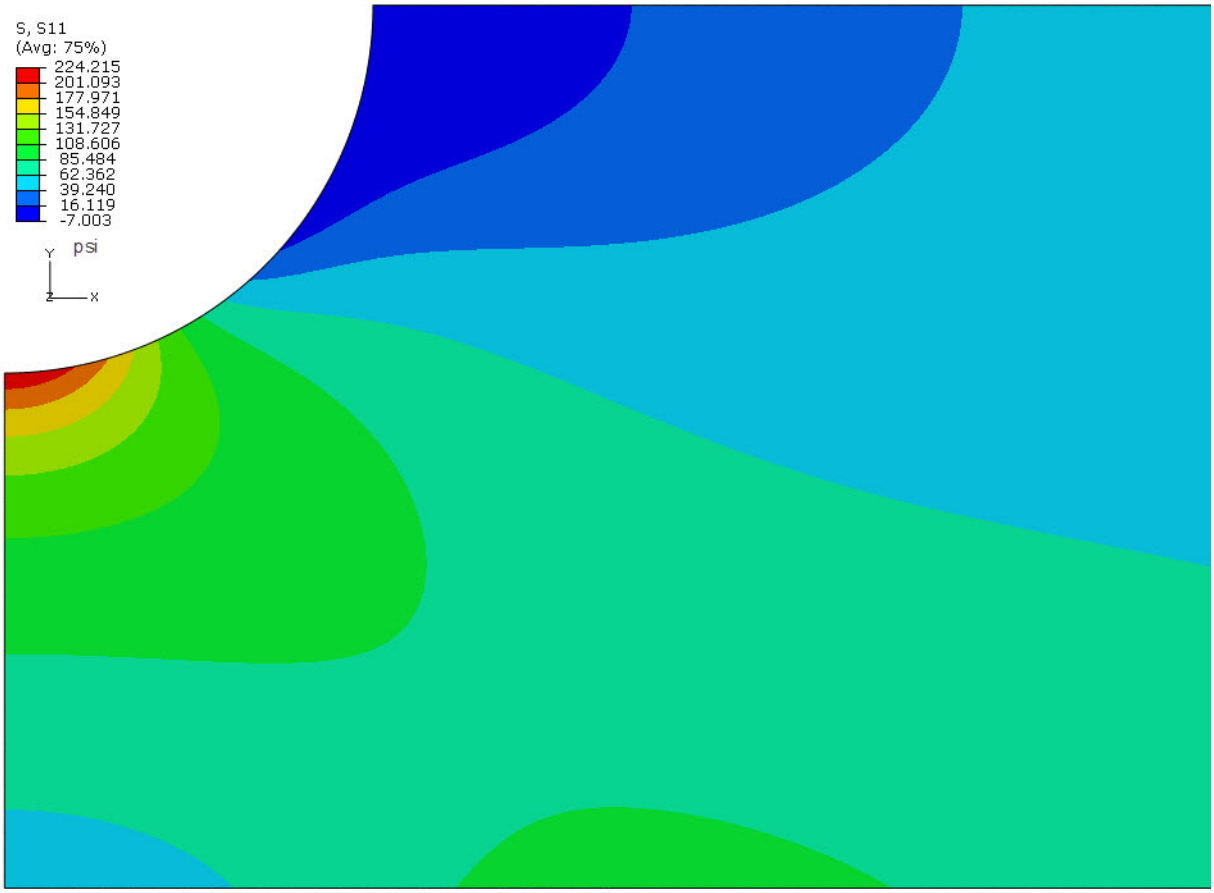
S, S11
(Avg: 75%)
224.215
201.093
177.971
154.849
131.727
108.606
85.484
62.362
39.240
16.119
-7.003
psi
Y
Z
X


S, S11
(Avg: 75%)
224.215
201.093
177.971
154.849
131.727
108.606
85.484
62.362
39.240
16.119
-7.003
psi
Y
Z
X

Edge Notch 1

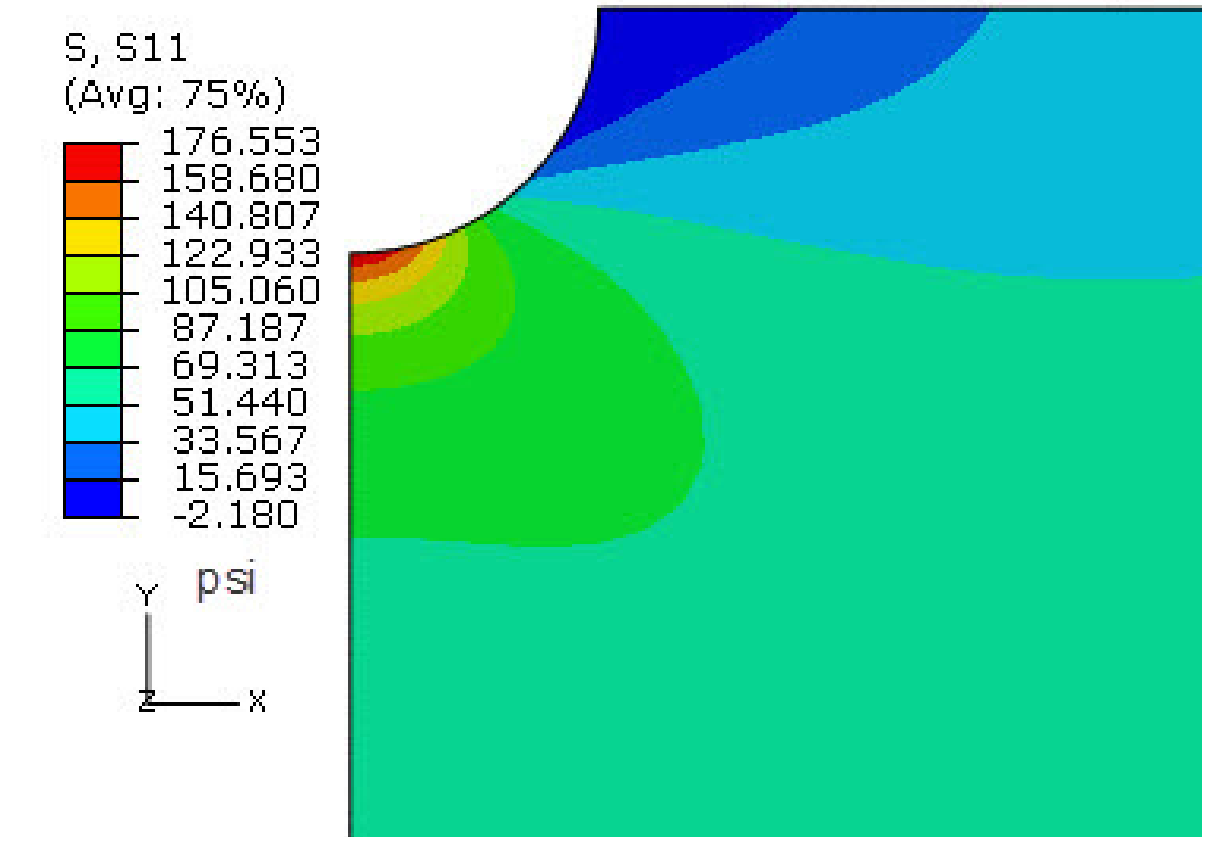
S, S11
(Avg: 75%)
176.553
158.680
140.807
122.933
105.060
87.187
69.313
51.440
33.567
15.693
-2.180
psi
Y
Z
X


S, S11
(Avg: 75%)
176.553
158.680
140.807
122.933
105.060
87.187
69.313
51.440
33.567
15.693
-2.180
psi
Y
Z
X

Edge Notch 2

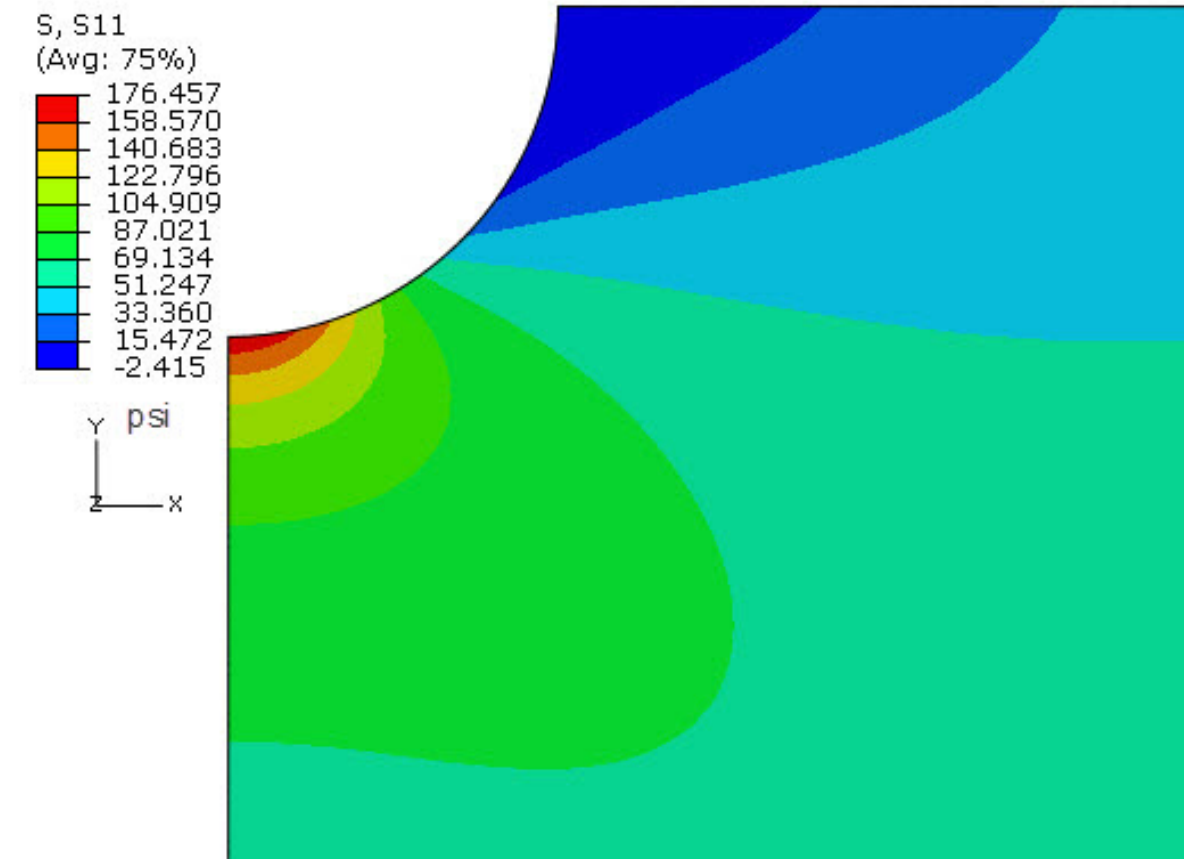
S, S11
(Avg: 75%)
176.457
158.570
140.683
122.796
104.909
87.021
69.134
51.247
33.360
15.472
-2.415
psi
Y
Z
X


S, S11
(Avg: 75%)
176.457
158.570
140.683
122.796
104.909
87.021
69.134
51.247
33.360
15.472
-2.415
psi
Y
Z
X

Edge Notch 3

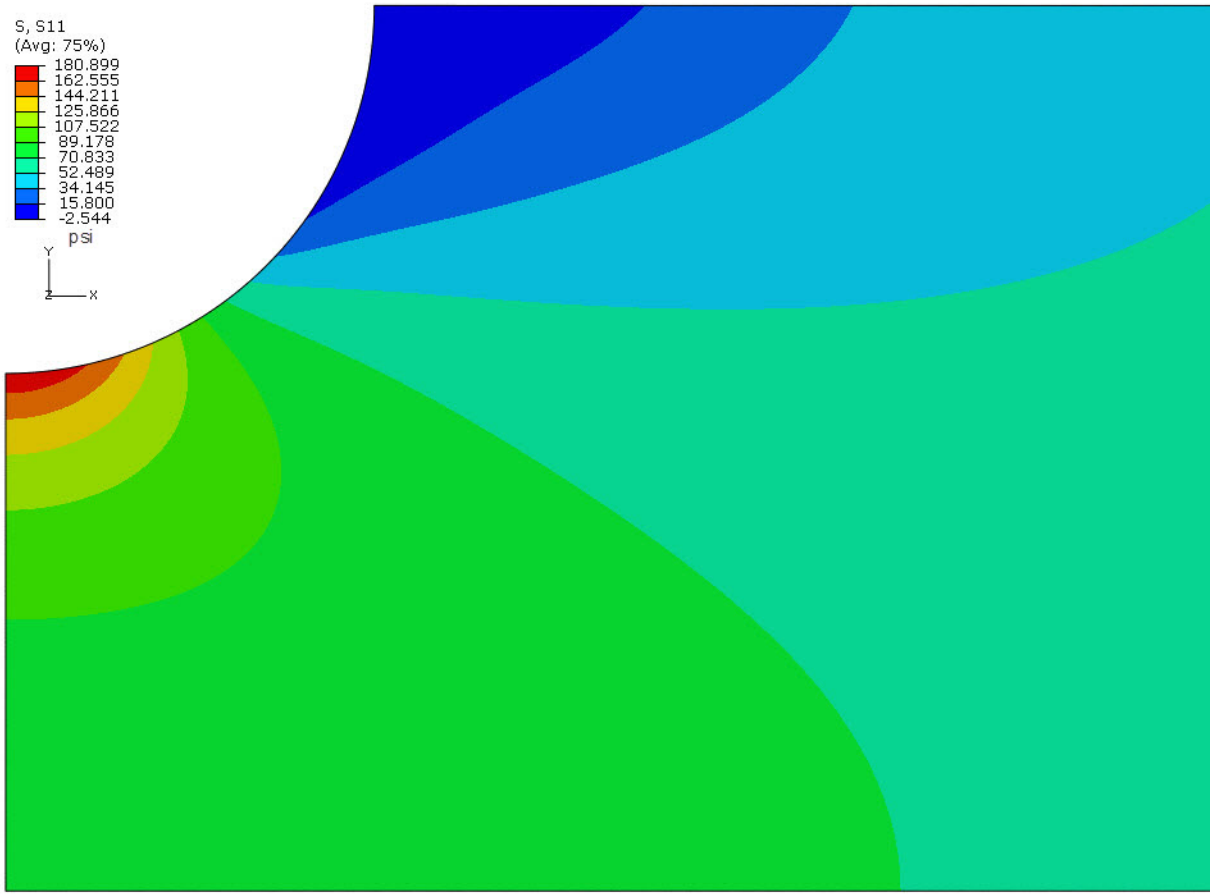
S, S11
(Avg: 75%)
180.899
162.555
144.211
125.866
107.522
89.178
70.833
52.489
34.145
15.800
-2.544
psi
Y
Z
X

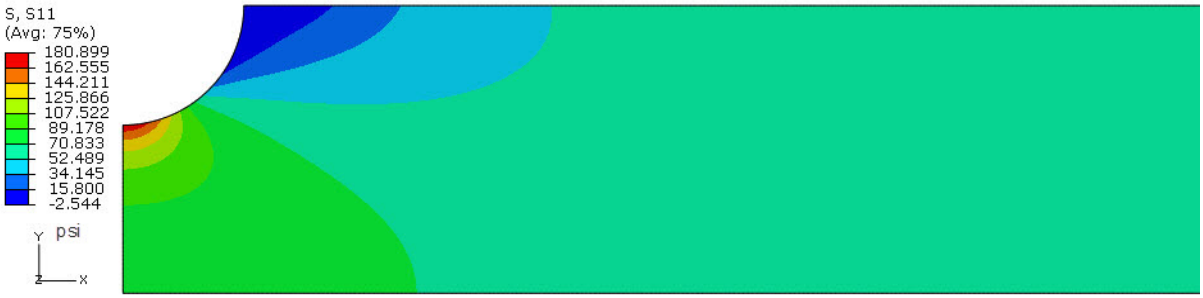
S, S11
(Avg: 75%)
180.899
162.555
144.211
125.866
107.522
89.178
70.833
52.489
34.145
15.800
-2.544
psi
Y
Z
X

Waist 1

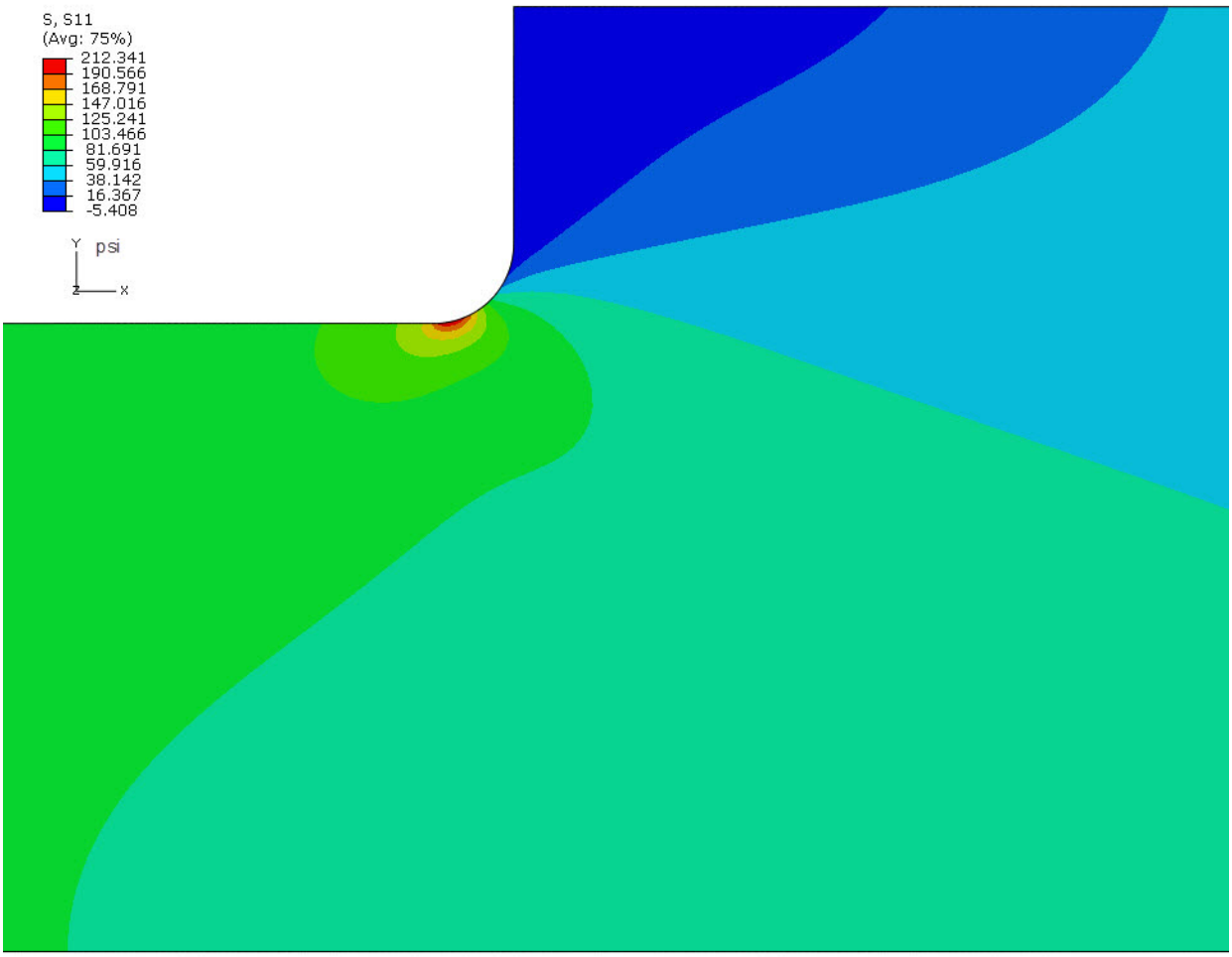
S, S11
(Avg: 75%)
212.341
190.566
168.791
147.016
125.241
103.466
81.691
59.916
38.142
16.367
-5.408
Y psi
Z X

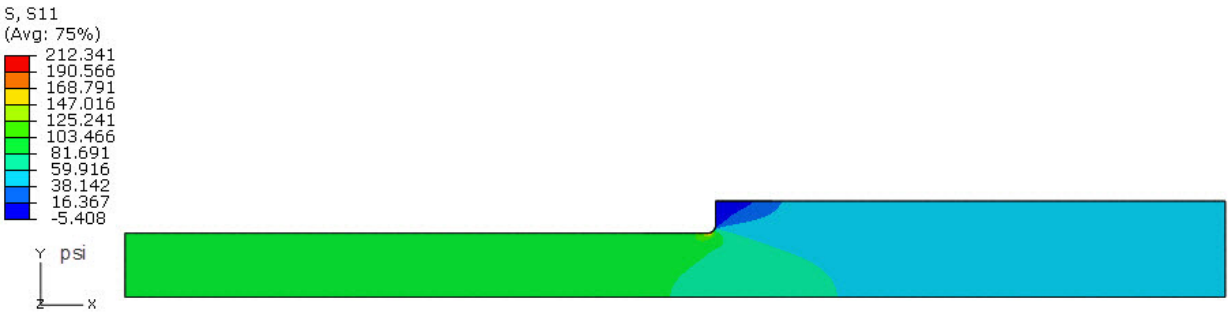
S, S11
(Avg: 75%)
212.341
190.566
168.791
147.016
125.241
103.466
81.691
59.916
38.142
16.367
-5.408
Y psi
Z X

Waist 2

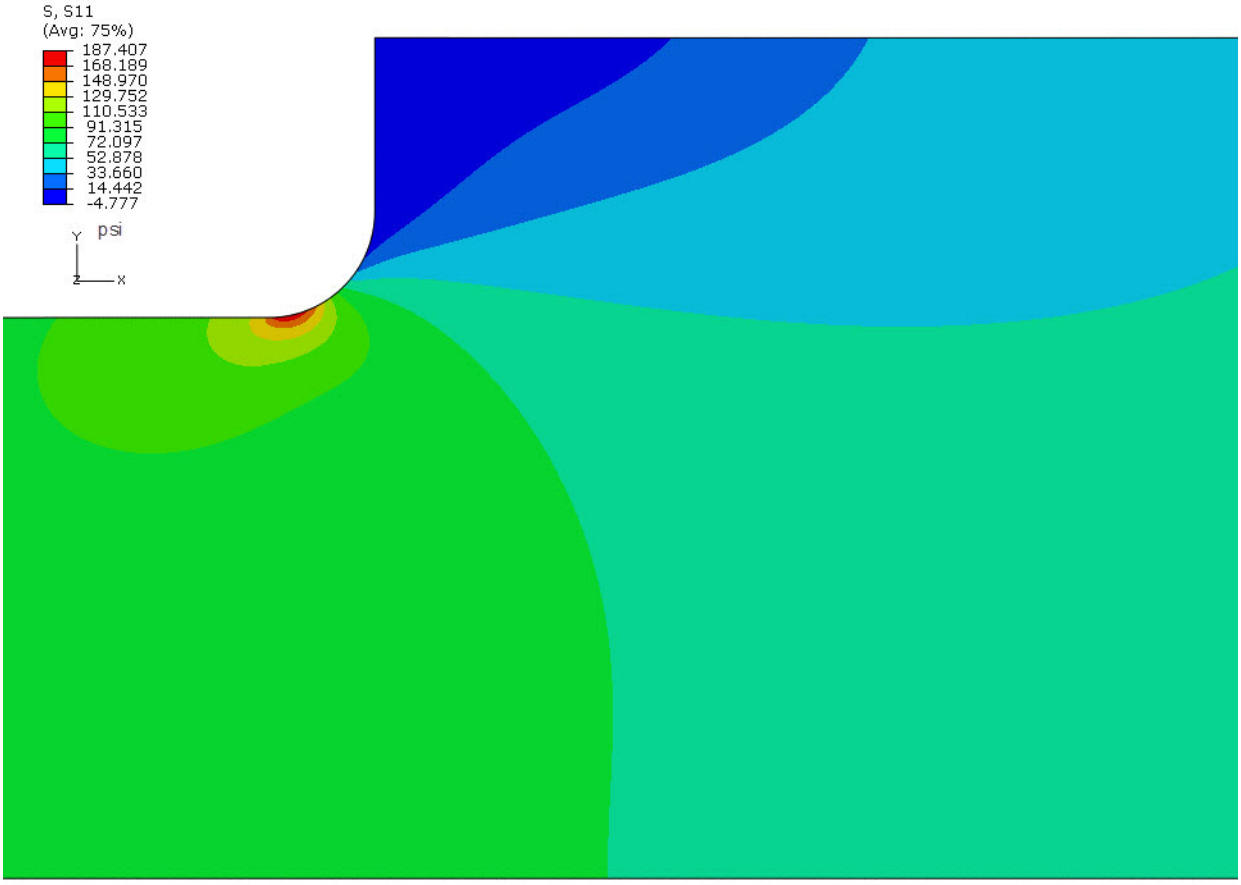
S, S11
(Avg: 75%)
187.407
168.189
148.970
129.752
110.533
91.315
72.097
52.878
33.660
14.442
-4.777
psi
Y
Z
X

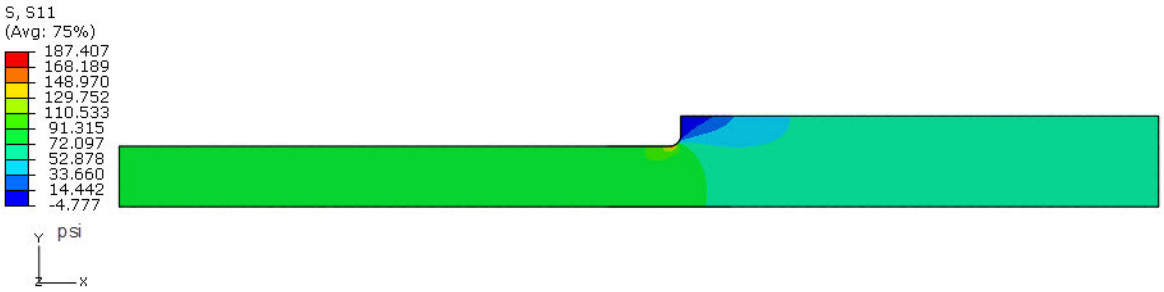
S, S11
(Avg: 75%)
187.407
168.189
148.970
129.752
110.533
91.315
72.097
52.878
33.660
14.442
-4.777
psi
Y
Z
X

Waist 3

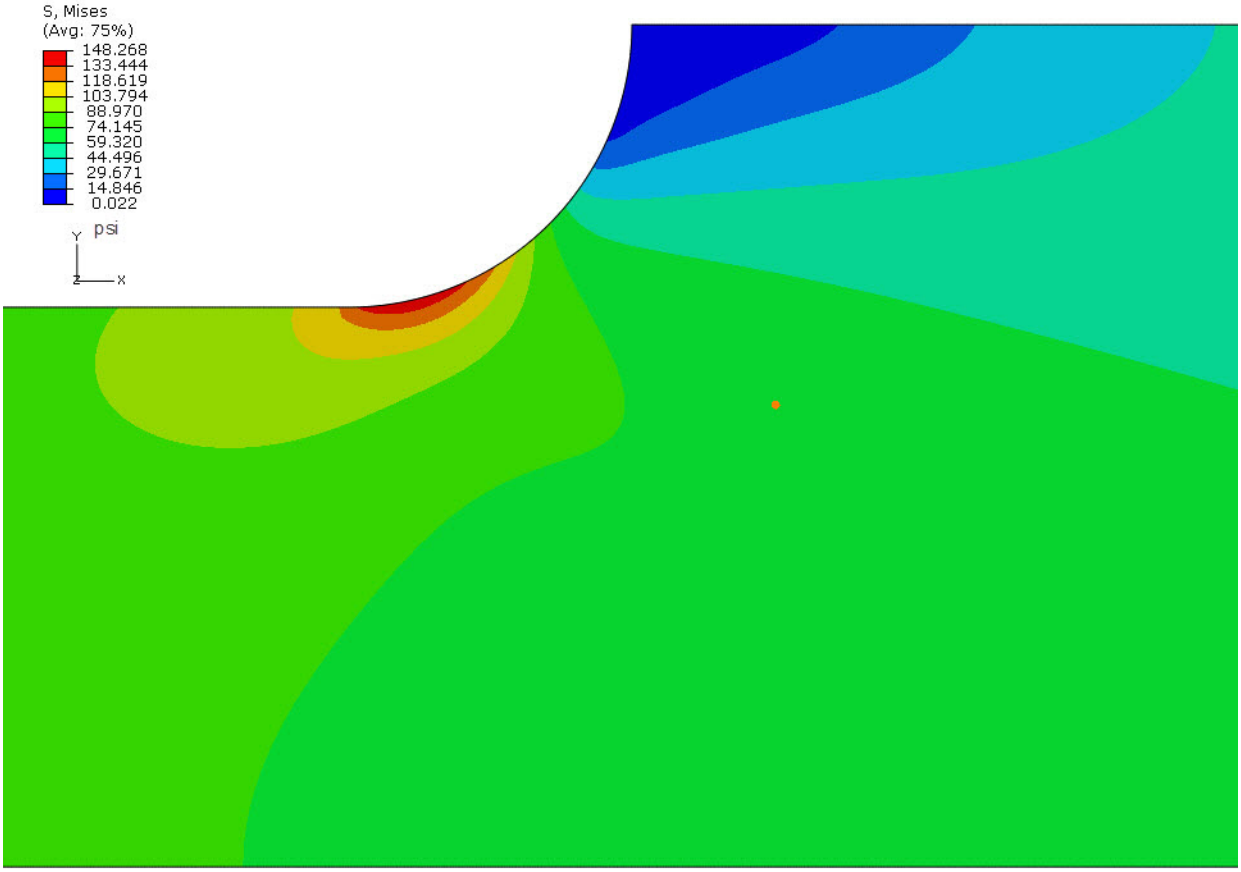
S, Mises
(Avg: 75%)
148.268
133.444
118.619
103.794
88.970
74.145
59.320
44.496
29.671
14.846
0.022
psi
Y
Z
X

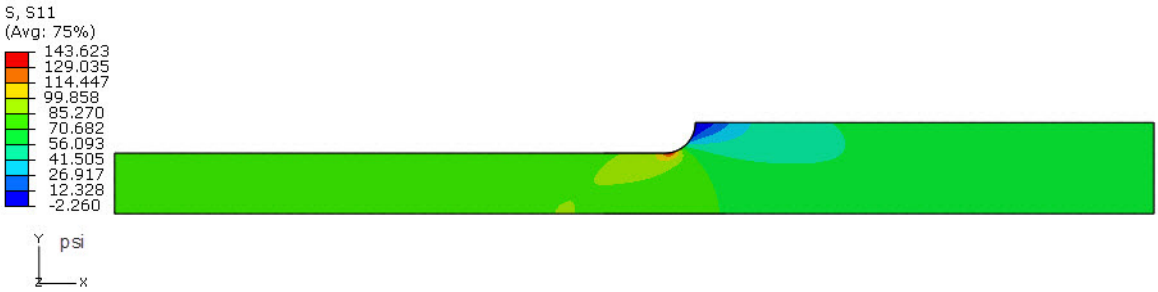
S, S11
(Avg: 75%)
143.623
129.035
114.447
99.858
85.270
70.682
56.093
41.505
26.917
12.328
-2.260
psi
Y
Z
X

A3 – Machining Process

For the results of this report, coupons had to be generated for physical testing. These specimens were machined from sheets of photoelastic sheets. The sheets are made of plastic PS-1A [4] with measured values for "K" Factor and "f" values that are used in the calculations and measured fringe plots. Before beginning with the manufacturing of the samples, a few items of concern must be addressed. The first is the material is sensitive to heat and thus should be kept at room temperature at all times. Second, due to the plasticity of the material the sheets should always be stored in a way that minimizes warping. Finally, stress and heat can be introduced during the machining process and as such the machining techniques should take this into account.

The sheets come in many sizes and may need to be reduced into a size more suitable for testing. The first step in creating the specimen is to cut the initial coupon from the photoelastic sheets. For this analysis the coupon size of choice was 10 in x 1.5 in. To obtain this initial size, the specimen was machined through several steps. The first step was to use a band saw [5] to cut the samples into strips that are 10 in long and 1.625 in wide. The added width is to allow the machining of the edges to remove any heat affected edge conditions from the band saw. At this point the specimens were then place in the machining fixture to reduce their width to the required 1.500 inches. It may be necessary to machine both long edges to remove the heat affected areas from both sides. The short ends were not machined as they are outside the area of interest.

The next phase of machining is the incorporation of specific features. All the samples have 2 holes 0.375 inches in diameter that are spaced 8.500 inches apart and on centerline long ways. A .375 in diameter center cut end mill was used to cut these holes. The end mill is plunged into the part to machine out the hole. An alternate method to creating these holes would be to drill to a slightly smaller size and then ream the hole to the correct size. For simplifications of machining the center cut end mill technique was used.

Finally, the geometry of interest is machined into the samples. The first set of samples has a hole placed at the center of the part. These holes are machined using the same techniques as described for the fixture holes but of their unique size. The second set of samples has an edge hole on either side of the sample on center and machined into the part exactly one half the diameter of the hole. The plunge cut method was also used on these samples.

The final set of samples has a necked region machined into it. These samples utilize a constant 1.000 inch internal width with differing corner radiuses. These samples required the most care need to machine of any of the samples. After several test runs it was found, the best way to machine the waist samples was to make several passes with a decreasing amount of material being removed. The final pass should remove no more than .001/.002 of an inch to obtain the desired shape. This becomes more important as the fillet radius r decreases as the resulting stress from machining begins to play a larger role in the analysis with respect to edge effects.

VITA

Matthew Lee Mauk

Candidate for the Degree of

Master of Science

Thesis: A REVIEW OF THE ACCURACY OF STRESS CONCENTRATION FACTORS

Major Field: Mechanical Engineering

Biographical:

Education:

Completed the requirements for the Master of Science in Mechanical Engineering at Oklahoma State University, Stillwater, Oklahoma in December, 2010.

Completed the requirements for the Bachelor of Science in Mechanical Engineering at Oklahoma State University, Stillwater, Oklahoma in 1999.

Name: Matthew Lee Mauk Date of Degree: December, 2010

Institution: Oklahoma State University Location: Stillwater, Oklahoma

Title of Study: A REVIEW OF THE ACCURACY OF STRESS CONCENTRATION FACTORS

Pages in Study: 42 Candidate for the Degree of Master of Science

Major Field: Mechanical Engineering

Scope and Method of Study:

Engineers rely on published results and data to be correct. If it wasn't, then they would be "reinvent the wheel" every time. This research will review the published results of stress concentration factors for semicircular edge notch geometry. It will be shown that two published sources show significantly different values for the stress concentrations of the semicircular edge notch geometry. Transverse holes and waist geometry will also be reviewed. The references will be compared with photoelastic models as well as FEA results.

Findings and Conclusions:

Results show that there exists a discrepancy between the published sources. There is a significant difference in the resulting stress concentration values for the same geometries. Photoelastic results were inconclusive based on error in the manufacturing and photoelastic analysis performed for this report and could have been responsible for errors in earlier sources. It is also noted that Finite Element Analysis is a viable alternative for characterizing the stress concentration values of geometry, as it has become a common tool for engineers.

ADVISER'S APPROVAL: Dr. James K. Good